ACS Photonics

Article

pubs.acs.org/journal/apchd5

# Strong Plasmonic Coupling between Graphene Ribbon Array and Metal Gratings

Bo Zhao and Zhuomin M. Zhang*

George W. Woodruff School of Mechanical Engineering, Georgia Institute of Technology, Atlanta, Georgia 30332, United States

Supporting Information

**ABSTRACT:** The collective oscillation of the massless electrons in graphene ribbons can interact with photons to create graphene plasmon polaritons. The resonance-induced absorption is critical in signal detection and energy harvesting applications. However, because of their atomic thickness, high absorptance is difficult to achieve with graphene ribbons alone. In this work, a hybrid plasmonic system composed of an array of graphene ribbons over a periodic metal grating is theoretically investigated. It is shown that the localized resonances, that is, magnetic polaritons, in metal gratings can couple with the plasmonic resonance in graphene ribbons, resulting in significantly enhanced absorption in graphene. Moreover, the coupling phenomenon depends on the width of the ribbons and the relative positions of the ribbon and the grating. The coupling between the grating and a continuous graphene monolayer sheet is also investigated and the results are compared to those with graphene ribbons. The findings of this work may facilitate the design of optoelectronic devices and metamaterials structures based on hybrid nanostructures and graphene.

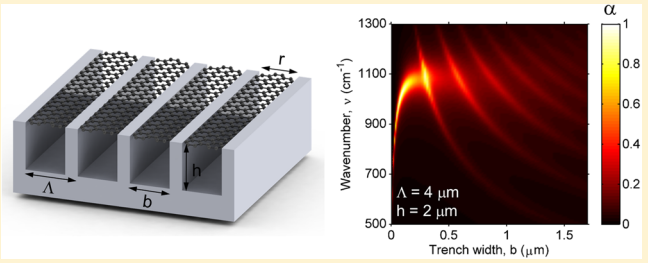


**KEYWORDS:** *graphene ribbon, magnetic polaritons, metal grating, plasmonic coupling, absorption enhancement*

Plasmons are collective oscillations of charge carriers and they play a critical role in optoelectronics and metamaterials applications. As an emerging two-dimensional (2D) material, graphene can support highly confined surface plasmons in the infrared region with relatively low loss compared to traditional plasmonic materials.[1−4] The strong coupling between the incident photon and the plasmons in graphene results in a polariton, which creates coherent absorption or transmission desired in applications such as energy harvesting and optical detection.[5−9] To excite polaritons with the photons incident from vacuum, graphene can be patterned into different periodic resonators such as ribbons,[10−13] disks,[14−17] and cross shapes.[18] In particular, graphene ribbon arrays[11−13] have attracted extensive attention recently. The electrons in the ribbons can be driven by external electromagnetic waves and oscillate inside the ribbon, forming surface plasmons that can induce a resonance absorption. Meanwhile, the optical properties of graphene ribbons can be tuned by controlling its chemical potential, resulting in tunable plasmonic resonances in the infrared region.[19−21]

In spite of these advantages, high resonance absorptance that is desired in the above-mentioned applications is difficult to achieve solely with graphene ribbon array due to its atomically thin thickness, especially for high-order resonances.[11] Thus, there is a need to explore novel ways that can enhance the plasmonic resonances in graphene structures like periodic ribbons. In the visible and near-infrared region, since the interband transitions of electrons dominate the optical response of graphene, its conductivity of graphene is a purely real quantity. In this case, graphene has no plasmonic responses but has very high loss. Thanks to this lossy property, the absorptance of graphene can be enhanced by placing graphene into an environment with strong electric fields. One way to generate such a strong electric field is to use plasmonic nanoantennas. Placing graphene at vicinity of them is capable to enhance the absorptance by 1 order of magnitude at the resonance frequency of the antenna, as has been experimentally demonstrated by many groups.[22−24] Another way is to utilize the localized polaritons in metal gratings and metamaterials, which can boost the absorptance of graphene from 0.023 to more than 0.8.[25−27] One of the prominent features of these methods is that, graphene does not affect the resonance conditions of the antenna or grating due to the absence of the plasmonic response in graphene. However, in the mid- and far-infrared, plasmons in graphene can strongly couple with the nanostructures and gratings to form a new hybrid plasmonic system.[28−30] For example, the plasmons in graphene can be launched and controlled by the plasmonic dipole resonance of metal nanoantennas.[31] This coupling phenomenon offers a novel route for the enhancement of plasmonic resonances in graphene and its nanostructures.

This work demonstrates that the localized polaritons, that is, magnetic polaritons (MPs), in deep metal gratings, can strongly couple with the surface plasmons in graphene sheets and ribbons. This coupling effect results in significant absorption

**Received:** July 23, 2015
**Published:** October 21, 2015





DOI: 10.1021/acsphotonics.5b00410
*ACS Photonics* 2015, 2, 1611−1618

enhancement in the mid-infrared region by boosting the intrinsic plasmonic resonance in graphene. The hybrid plasmonic system described here differs largely from the previous works[25,26] where the interband transitions dominate graphene conductivity in the near-infrared region. When coupled with graphene plasmons, the MP may be modified to have a different resonance frequency from that of the plain gratings due to the inductance effect of graphene. The metal grating, on the other hand, alters the dispersion of the graphene plasmons by changing the phase shift of the plasmon waves at the edges of the ribbons. As a result, the absorption peak location as well as magnitude can be tuned by either changing the grating geometries or controlling the chemical potential of graphene. Furthermore, the placement of the ribbons with respect to the gratings controls the coupling strength. The chemical potential plays an important role to couple or decouple MPs with graphene plasmons. It is also shown that continuous graphene can enable the same coupling phenomena as graphene ribbons. This may offer a practical way to experimentally realize the plasmonic coupling between graphene ribbons and gratings.

## RESULTS AND DISCUSSION

The geometric arrangement of the graphene ribbon-grating hybrid structure is illustrated in Figure 1a. The grating is periodic in the $x$-direction and extended infinitely in the $y$-direction. It has a period $\Lambda$, trench width $b$, and grating height $h$. Unless specified, the geometries are fixed as $\Lambda = 4\ \mu$m, $b =$ 300 nm, and $h = 2\ \mu$m. The width of the ribbons is $r$ ($r \leq b$); noting that when $r = b$, the edges of ribbons will be in physical contact with the grating as shown in the schematic. The cases where they are not in contact will be discussed later. The ground plane is assumed to be thick enough to be treated as opaque. The grating and ground plane are chosen to be silver (Ag) whose optical constants is calculated by a simple Drude model, which works well in the mid-infrared.[32] The optical properties of graphene include the contributions from the interband and intraband transitions.[33] In the mid- and far-infrared region, the intraband transitions dominate and the conductivity can be approximately expressed in a Drude-like model:[1]

$$\sigma_s = \frac{e^2\mu}{\pi\hbar^2}\frac{\tau}{1 - i\omega\tau} \quad (1)$$

where $e$ is the charge of an electron, $\mu$ is the chemical potential, $\hbar$ is the reduced Planck constant, $\omega$ is the angular frequency, and $\tau$ is the relaxation time. The chemical potential can be tuned by electrical gating or chemical doping and, thus, offering an active way to control the optical properties of graphene ribbons. In this study, otherwise specified, $\mu = 0.3$ eV and $\tau = 10^{-13}$ s are used. For transverse magnetic (TM) waves, the oscillating magnetic field in the $y$-direction induces a current loop around the trench of the grating, which generates a highly localized magnetic field inside the trench and forms an MP.[32,34] The absorptance spectra of the plain and ribbon-covered structure are shown in Figure 1b at normal incidence. For the plain grating, the MP resonance is at 1041 cm$^{-1}$ with an absorptance of 0.35. After coving ribbons on the grating, the absorptance is boosted to 0.94 and the resonance shifts to 1086 cm$^{-1}$, indicating a strong coupling between graphene and the grating. The spectrum of the free-standing ribbon array without the grating is also given in Figure 1b for comparison. In this

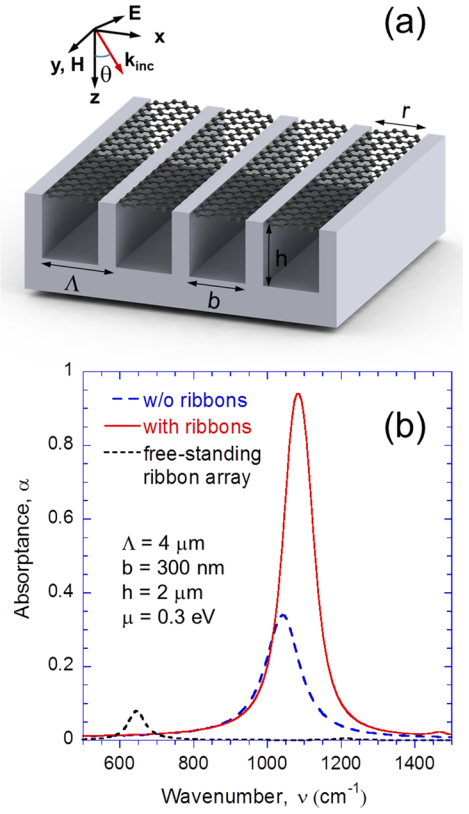


**Figure 1.** (a) Schematic of the hybrid grating-graphene ribbon plasmonic structure under plane wave incidence. Here, $\Lambda$, $h$, and $b$ are the period, height, and trench width of the grating as well as the graphene ribbon array, and $r$ is the width of the ribbon. When $r = b$, the ribbon edges are in contact with the grating. (b) Normal absorptance spectrum for a plain Ag grating, a free-standing ribbon array, and a ribbon-covered grating ($r = b$) for TM waves. The geometric parameters of the grating and graphene ribbons, along with the chemical potential of graphene used for the calculation are given in the figure.

case, the ribbon plasmon gives rise to a small absorption peak around 650 cm$^{-1}$. It will be discussed later that the grating can alter the dispersion of the graphene plasmons by changing the phase shift of the plasmon waves at the edges of the ribbons.

The resonances with and without graphene can be modeled using the equivalent circuit method, which has been successfully applied to predict the resonance condition of various nanostructures.[35,36] In this method, metal and dielectric are treated as inductors and capacitors, respectively, forming an inductor-capacitor (LC) circuit. The resonance frequency of the polaritons can then be obtained by solving the natural frequency of the LC circuit. The details of the models used in this work are explained in Methods. The model yields a resonance frequency of 1047 cm$^{-1}$ without the graphene ribbon and 1093 cm$^{-1}$ with the graphene ribbon. The red shift caused by graphene is because graphene ribbons serves as an inductor across the trench that lowers the total inductance in the circuit. However, the reason for the absorptance enhancement cannot be explained by the LC model that does not consider loss. To further elucidate the enhanced absorption, the ribbon plasmon is discussed next.

The surface plasmons for TM waves can propagate along the $x$-direction with low loss in a continuous, free-standing


DOI: 10.1021/acsphotonics.5b00410
ACS Photonics 2015, 2, 1611−1618

graphene layer. The dispersion of the graphene surface plasmon satisfies

$$\frac{\varepsilon_1}{\sqrt{k_{GSP}^2 - \varepsilon_1 k_0^2}} + \frac{\varepsilon_2}{\sqrt{k_{GSP}^2 - \varepsilon_2 k_0^2}} = -\frac{i\sigma_s}{\omega\varepsilon_0} \quad (2)$$

where $k_0 = \omega/c_0$ is the vacuum wave vector, with $c_0$ being the light speed in vacuum, $k_{GSP}$ is the wave vector for the plasmon, $\varepsilon_0$ is the permittivity of vacuum, and $\varepsilon_1$ and $\varepsilon_2$ are the dielectric functions of the media that are on each side of graphene. If graphene is surrounded by the same medium, that is, $\varepsilon_1 = \varepsilon_2$, then the dispersion can be simplified as[37]

$$k_{GSP} = \frac{\omega}{c_0}\sqrt{\varepsilon_1 - \frac{4\varepsilon_0}{\sigma_s^2\mu_0}} \approx \frac{2i\omega\varepsilon_0}{\sigma_s} \quad (3)$$

where $\mu_0$ is the vacuum permeability. The plasmons in ribbons, however, cannot propagate freely but are reflected back on the ribbon edges with a phase shift $\Delta\varphi$. The reflection of plasmon waves in various graphene nanostructures has been previously studied.[38,39] Recently, it is found that this phase shift is $\pi/4$ for free-standing ribbons in vacuum.[40,41] Once the reflection phase shift is known, the resonance in suspended graphene ribbons can be described by a Fabry-Pérot model:

$$\Delta\varphi + \mathrm{Re}(k_{GSP})r = m\pi \quad (4)$$

where integer $m$ denotes the resonance order and Re takes the real part of the complex quantity. By substituting eq 3 into eq 4, the resonance condition of suspended ribbons in vacuum ($\varepsilon_1 = \varepsilon_2 = 1$) can be expressed explicitly as[41]

$$\omega = \sqrt{\frac{e^2\mu(m - \Delta\varphi/\pi)}{2\varepsilon_0\hbar^2 r}} \quad (5)$$

At normal incidence, the plasmon initiated from the two edges of the ribbon are out of phase, and thus, only the plasmons associated with odd $m$s can show up. The plasmons with even $m$s can only occur at oblique incidence since in-phase plasmons can be excited from the two edges.[41]

Figure 2 shows the absorptance ($\alpha$) contour of a suspended graphene ribbon array at normal incidence obtained by using rigorous coupled-wave analysis (RCWA). The dashed lines, from bottom to top, are the predictions from eq 5 with $m$ = 1, 3, 5, and 7, respectively. The frequency of the resonance is inversely proportional to $\sqrt{r}$. Note that the highest absorptance occurs for $m$ = 1 at $r \approx 2$ $\mu$m with a value near 0.35. For the other branches with higher orders, the absorption by graphene ribbons is rather small. As will be shown next, metal gratings can significantly enhance these ribbon resonances.

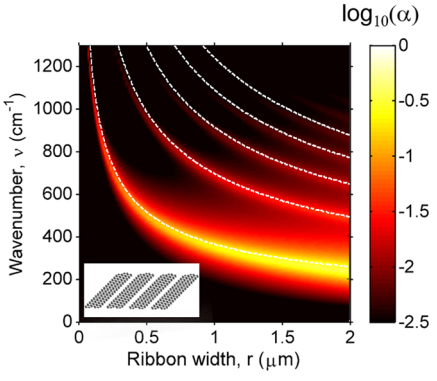


**Figure 2.** Absorptance contour of free-standing graphene ribbon arrays with $\Lambda$ = 4 $\mu$m and $\mu$ = 0.3 eV, in terms of the frequency and the ribbon width $r$, at normal incidence. The dashed lines are calculated from eq 5 using $\Delta\varphi = \pi/4$.

Figure 3 compares the absorptance contours at normal incidence for four different configurations versus the trench width. The plain gratings support MP resonances in the considered frequency range, as shown in Figure 3a. The frequency of the MP increases with $b$ and reaches an asymptotic value when $b$ > 0.25 $\mu$m. The absorptance diminishes at large trench widths due to the poor coupling of the evanescent waves between the two side walls in the trench.[32] The dot markers are the predictions of the LC model. The absorptance contour stays the same if the graphene ribbon is covered only on the ridges of the grating, as shown in Figure 3b. The graphene ribbons appear to have no effect on the resonance since they are in contact with the metal on one side. On the contrary, if the ribbons are suspended above the trench openings, as the case in the inset of Figure 3c, the plasmonic resonances of the ribbons show up and the absorptance becomes more plentiful. The bright bands with a dependence of $1/\sqrt{b}$ are caused by the plasmons in ribbons. Note that when the grating trench is changing, $r$ changes accordingly so that the edges of the ribbons are always in touch with Ag. Although the shape of these bands is similar to those in Figure 2, the ribbon resonances in Figure 3c cannot be predicted with eq 5 using the reflection phase shift $\pi/4$. In fact, since the edge is touched with Ag instead of vacuum, the tangential component of the electric field ($E_z$) at the edges need to vanish at the boundary due to the high conductivity of Ag, resulting in a phase shift of $-\pi$ for the plasmon waves. This can be further justified by the excellent agreement between the

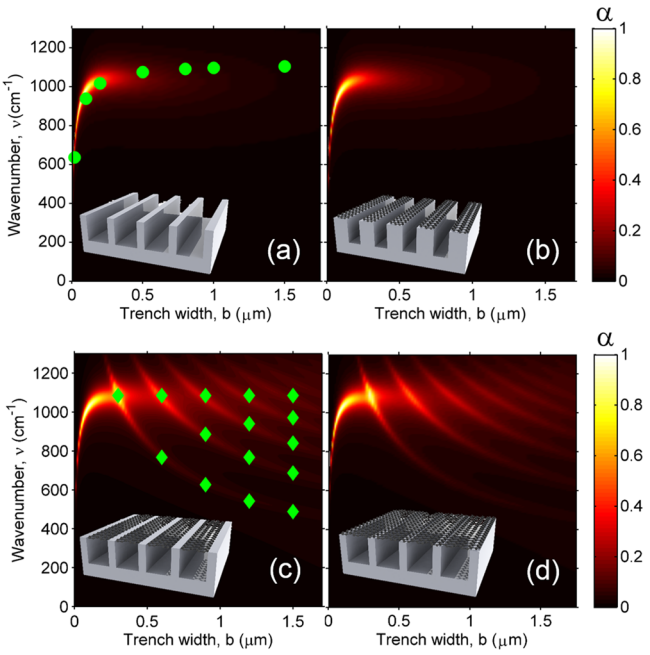


**Figure 3.** Compilation of the absorptance contours for four different structures when $\Lambda$ = 4 $\mu$m, $h$ = 2 $\mu$m, and $\mu$ = 0.3 eV are fixed, while $b$ changes: (a) plain Ag grating; (b) graphene ribbons covering the Ag grating ridges; (c) graphene ribbons covering the trench opening ($r = b$); and (d) continuous graphene sheet covering the whole grating. The round markers are the predictions of eq 11 and the diamond markers are the predictions of eq 5.



DOI: 10.1021/acsphotonics.5b00410
ACS Photonics 2015, 2, 1611−1618

simulation and the prediction results of eq 5 with $\Delta\varphi = -\pi$, which is demonstrated in Figure 3c. Note that the plasmons are all associated with odd $m$s since the incidence is normal.

Covering the grating by a continuous graphene, as illustrated in Figure 3d, yields the same absorptance contour as Figure 3c. Again, the portion of the graphene on the ridges has little contribution on the resonance. Thus, in terms of absorptance, continuous graphene is equivalent to a periodic ribbon array suspended over the grating trenches. Since the fabrication of the structure with continuous graphene on grating can be realized with the existing fabrication technique,[28] it provides a realistic way to experimentally achieve the coupling between MP and plasmons in ribbon array. The branches for ribbon plasmons are intersected with the MP and the absorptance at the intersection points are enhanced significantly, indicating a strong coupling between the MP and the ribbon plasmons. The spectrum at $b = 0.3$ $\mu$m contains a strongly coupled resonance at $\nu = 1086$ cm$^{-1}$ and has been shown in Figure 1b. The absorption by the graphene ribbons, to be shown next, can be significantly enhanced at this resonance.

Figure 4 illustrates the power dissipation profile at the coupled resonance when $b = 0.3$ $\mu$m and the calculation details

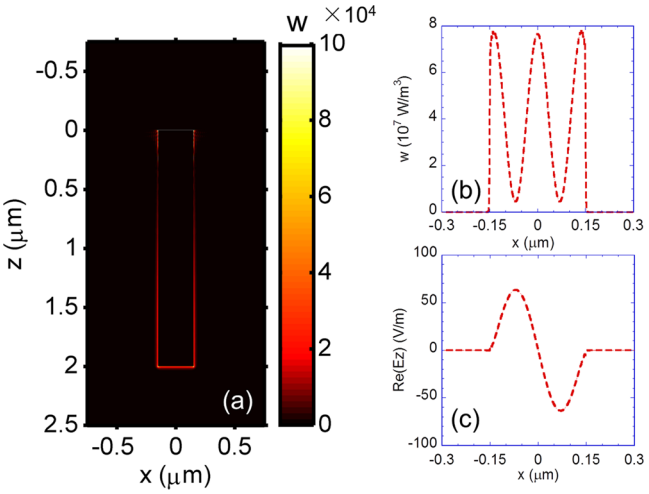


**Figure 4.** Power dissipation density at the coupled resonance when $b = 0.3$ $\mu$m: (a) for the whole structure and (b) across the middle of the graphene. (c) Modulus of $E_z$ at the location beneath the graphene inside the trench.

are given in Methods. The grating is covered with a continuous graphene. The absorption in grating at the coupled resonance, as demonstrated in Figure 4a, is mainly confined at the surface of the trench. This is due to the short penetration depth of electric field in the metal that is only about 10 nm. The absorption in the graphene, however, is concentrated in the portion that is on the trench opening. This further justifies that the graphene in contact with the grating ridges plays little role on the resonance. Note that the scale bar is chosen in a way such that the absorption of the grating can be clearly seen. The detailed absorption distribution in graphene is shown in Figure 4b according to the dissipation density along the middle of the graphene layer. Due to the interference effect of the plasmonic waves, the dissipation exhibits a standing-wave pattern at the trench opening and is symmetric with respect to the $x = 0$ plane. Note that the electric field is dominated by its $x$-component in the graphene. The portion of energy absorbed by the graphene is calculated to be 72%, which is greatly boosted from 8% for a free-standing graphene ribbon with $r = 0.3$ $\mu$m when the first-order plasmon is excited at normal incidence, as shown in Figure 2. The last figure is the real part of $E_z$ close to the lower surface of graphene layer at the coupled resonance. Note that $E_z$ vanishes at the edges. The phase shift across the trench, $\mathrm{Re}(k_{GSP})r$, equals $2\pi$, in agreement with eq 4 when $m = 1$.

Figure 5a illustrates the contour plot of the absorptance when the incidence angle is fixed at 50° with varying trench

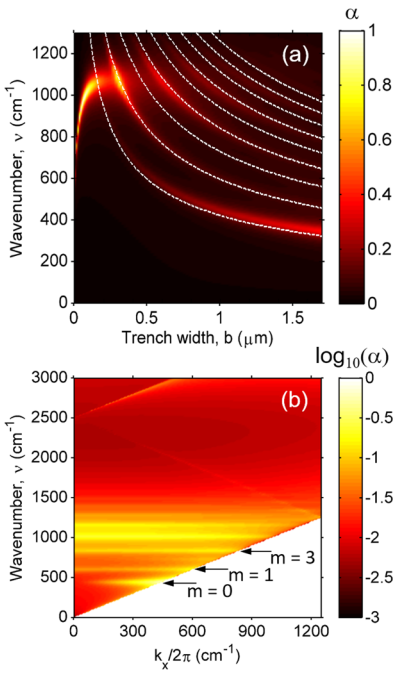


**Figure 5.** (a) Absorptance contour at $\theta = 50°$ for the structure with ribbons covered at the trench opening ($r = b$), where the dashed lines are the predictions from eq 5. (b) Absorptance contour for a grating with $b = 1$ $\mu$m showing dependence on the transverse wave vector.

width while the ribbon width remains the same as the trench width ($r = b$). Compared with Figure 3c, Figure 5a exhibits additional bright bands corresponding to the even-order plasmons. The predictions from eq 5 are shown as dashed lines, which agree well with the direct simulation. Moreover, the resonance frequencies of the MPs and the ribbon plasmons, compared to the normal incidence case, change little at $\theta = 50°$ due to their localized resonance feature. Figure 5b illustrates the absorptance contour of a grating with $b = 1$ $\mu$m when the $x$-component of the wave vector of the incidence, $k_x = \sin\theta(\omega/c_0)$, changes. The folded bright bands are the surface plasmon polaritons between the interface of silver grating and the vacuum.[34] The ribbon plasmons associated with odd $m$s can be excited at all incident angles while the even ones show up only at the oblique incidence. However, the absorptance bands are all flat, indicating that they are insensitive to the incidence angle. The MP resonance at around 1000 cm$^{-1}$ is also insensitive[32] to $k_x$ so that it can omnidirectionally couple with the plasmons in the ribbons that are around the same frequency.

The previous discussions are for the scenarios where the graphene ribbons are in contact with the top surface of the Ag grating, that is, the elevation between graphene ribbons and the grating ($t$) is zero. In the applications where the chemical potential of graphene needs to be tuned by electrical gating, a


DOI: 10.1021/acsphotonics.5b00410
ACS Photonics 2015, 2, 1611−1618

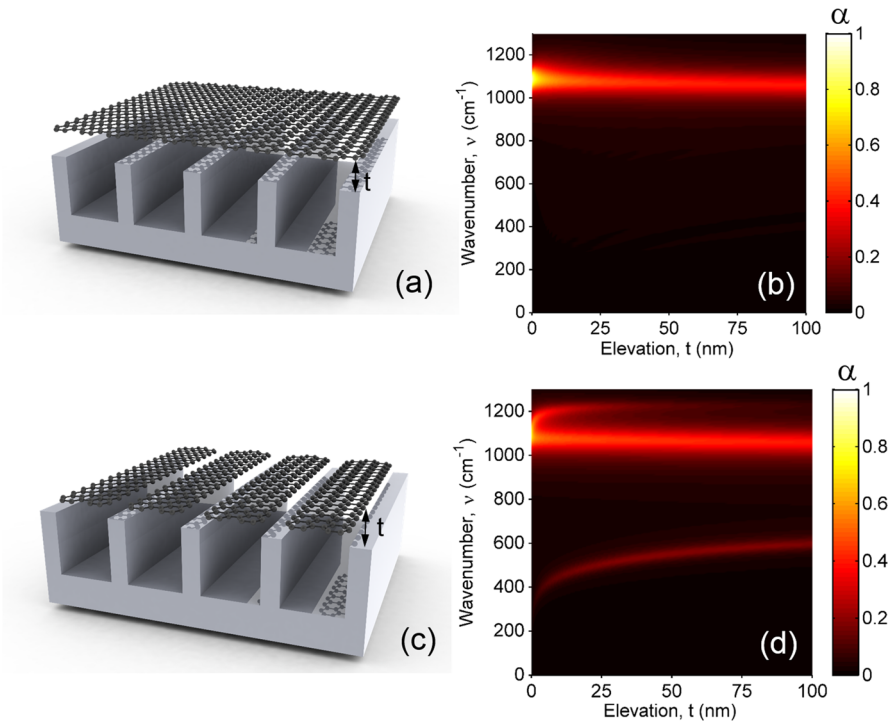


**Figure 6.** (a) Graphene above Ag grating with an elevation $t$. (b) Absorptance contour for the structure shown in (a) when $t$ changes. (c) Graphene ribbons above Ag grating with an elevation $t$. (d) Absorptance contour for the structure shown in (c) when $t$ changes.

dielectric layer may be inserted between the grating and graphene to prevent the flow of electrons between them.[19] It is expected that the coupling strength may deteriorate or even vanish when $t$ increases. Figure 6 demonstrates this transition for normal incidence with $b = 0.3$ $\mu$m, where the graphene is lifted in vacuum with respect to the ridges of the grating (without using a dielectric layer). For continuous graphene shown in Figure 6a, the coupling strength deteriorates once the graphene sheet detaches from the grating, as shown in Figure 6b. The resonance frequency shifts slightly to lower frequencies when $t$ increases. When $t$ exceeds about 1.5 $\mu$m, the asymptotic value is reached at 1041 cm$^{-1}$, which is the frequency of the MP resonance for a plain grating, though not shown here.

The scenario becomes more complicated for the ribbon covered grating shown in Figure 6c. Three resonance branches are identified on Figure 6d. The coupled resonance, which is the middle branch, degenerates to the MP resonance of the plain grating at 1041 cm$^{-1}$ when $t$ increases, similar to the previous continuous graphene case. The upper and lower branches are associated with the plasmons in the ribbon array. When the ribbons are in contact with the grating, the strong resonance at 1086 cm$^{-1}$ is due to the coupling of the MP in grating and the plasmon in ribbons with $m = 1$ and $\Delta\varphi = -\pi$. Once the ribbon array is detached, the phase shift of the plasmon upon reflection at the edges is no longer $-\pi$. Due to the sudden change of $\Delta\varphi$, the plasmon in ribbons associated with $m = 1$ shifts to lower frequencies and create the lower branch and the plasmon associated with $m = 3$ generates the upper branch. This also explains why the lower branch disappears at small $t$ values. The graphene ribbon plasmons recover the case of a free-standing ribbon array when $t$ is very large. The asymptotic resonance frequencies for the upper and lower branches are 1272 and 664 cm$^{-1}$, respectively, which are obtained from eq 5 using $\Delta\varphi = \pi/4$. Thus, the phase shift is dependent on $t$. Due to the effect of grating, the two branches gradually approach the asymptotic values as the elevation increases. Note that if the ribbons are moved downward into the grating trench, the coupled resonance will not split but the absorptance will decrease. This is discussed in detail in the Supporting Information, where a zoomed-in view of Figure 6d is also given to better show the resonance at small elevations.

The coupling phenomena can also be significantly modified by the width of the ribbon. Figure 7a illustrates the structure where $r$ is narrower than the trench width, which is fixed at 0.3 $\mu$m. The graphene ribbons are centered at the trench openings

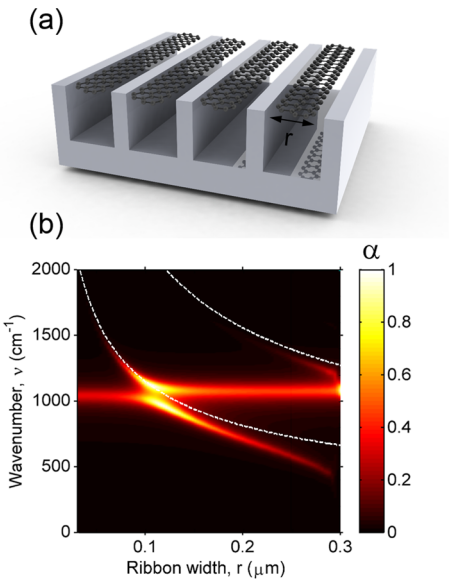


**Figure 7.** (a) Graphene ribbons covered Ag grating with ribbon width $r < b$. (b) Absorptance contour for the structure shown in (a) when $r$ changes.



DOI: 10.1021/acsphotonics.5b00410
ACS Photonics 2015, 2, 1611−1618

with $t = 0$. The continuous absorption branch for the graphene plasmon associated with $m = 1$ splits when crossed with the MP branch, as shown in Figure 7b. There appears to be mode splitting or anticrossing between the MP and ribbon plasmon branches near $r = 0.11$ $\mu$m, when the ribbon edges are not in contact with the grating. Subsequently, two hybrid polaritons at different energies can be excited for $0.09 < r < 0.13$ $\mu$m. On the contrary, as shown in Figure 3c or d and Figure 5a, the MP and ribbon plasmon branches cross each other, when the ribbons are in contact with the gratings. The exact reason for this difference needs further investigation. There exists an upper branch that corresponds to $m = 3$, as shown in Figure 7b. The dashed lines represent the predictions of eq 5, with $\Delta\varphi = \pi/4$ for $m = 1$ (lower branch) and 3 (upper branch), respectively. It can be seen that the predicted ribbon plasmon dispersions agree well with the simulation for a small $r$ but deviate when $r$ gets larger. This deviation may be caused by the change of reflection phase shift, which is $\pi/4$ at small $r$ and varies when the edges of the ribbons get closer to the silver trench walls. The $m = 1$ branch disappears at $r \approx 0.3$ $\mu$m since $\Delta\varphi$ approaches $-\pi$, and similar reason holds for $t = 0$ in Figure 6d.

Besides the geometry factors, the chemical potential of graphene can also modify the coupling picture by changing the dispersion of the graphene plasmons. For example, Figure 8 shows the absorptance spectra for the structure shown in Figure 1a with various $\mu$. The case when $\mu = 0.3$ eV corresponds to the solid spectrum in Figure 1b. If $\mu$ changes to 0.28 or 0.32 eV, the ribbon plasmon shifts to a slightly lower or higher frequency, respectively, and the coupling strength decreases as the peak absorptance becomes lower. When $\mu$ further decreases to $\mu = 0.2$ eV, two bumps at 871 and 1164 $cm^{-1}$ occur that are due to the plasmons associated with $m = 1$ and 3, respectively. However, neither of them can couple with the MP, whose absorptance drops down to about 0.4. Similarly, at $\mu = 0.5$ eV, the plasmon in ribbons associated with $m = 1$ moves to 1412 $cm^{-1}$ and totally decouples with the MP. Note that there is a slight shift of MP resonance at different $\mu$ and this can be understood with the equivalent LC model.[42] Therefore, the chemical potential can be tuned to control plasmons in the ribbons to couple or decouple with the MP resonance in the grating. Note that if the interband transitions dominate the conductivity of graphene, the ribbon will couple with MPs in grating without affecting the resonance frequency of the MPs.[25,26] Thus, the coupled resonance is difficult to be tuned by the chemical potential. More detailed discussions are provided in the Supporting Information.

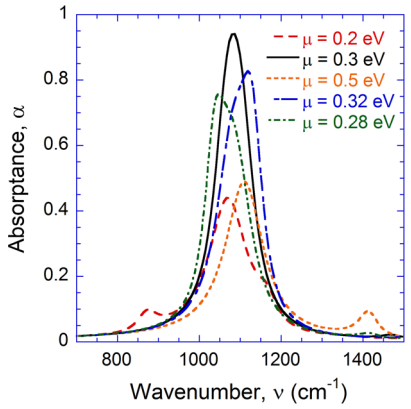


**Figure 8.** Absorptance spectra of the structure shown in Figure 1a with different graphene chemical potentials.

## CONCLUSION

This work demonstrates that the MPs in Ag grating can couple with the plasmons in ribbon arrays, resulting in greatly enhanced absorption of ribbons. The graphene ribbon acts as an inductor in the equivalent LC circuit and shifts the MP resonance to higher frequencies. In contrast to the free-standing ribbon arrays, the reflection phase shift becomes $-\pi$ when the ribbon edges are in contact with silver. The coupling effect deteriorates when the ribbons are elevated above the gratings. The width of the ribbon can be adjusted to create two coupled resonances at the same time. Furthermore, the chemical potential of graphene may be tuned to control the coupling between the two resonances. It is noted that graphene covered ridges has negligible effect and the resulting absorptance spectrum for a continuous sheet of graphene covered gratings is essentially the same as graphene ribbon arrays at the trench openings. Findings from this study shed light on the plasmonic coupling between graphene ribbons and metal gratings and may facilitate the design of next-generation optoelectronic systems based on graphene nanostructures.

## METHODS

**Numerical Modeling.** Continuous graphene sheet can be simulated as a thin isotropic layer with an effective dielectric function that is related to its conductivity. Here, the thickness of the graphene layer is chosen as $\Delta = 0.3$ nm and the dielectric function is then obtained based on $\varepsilon_{eff} = 1 + i\sigma_s/(\varepsilon_0\omega\Delta)$.[37] RCWA is used to calculate the reflectivity of the structure as well as the field distribution. The MATLAB code used has been published online.[43] However, graphene ribbons are difficult to be modeled in a similar way due to convergence issues.[44] Here, an approximate boundary condition is used[44] in which the graphene ribbons is treated as a period surface conductivity pattern that modifies the boundary conditions of the magnetic field. The absorptance for the whole structure is obtained from one minus the reflectivity since the grating ground plane is opaque and no energy is transmitted. In order to know the local absorption, the power dissipation density is calculated[25,45]

$$w(x, z) = \frac{1}{2}\varepsilon_0\omega\varepsilon''(x, z)|\mathbf{E}(x, z)|^2 \tag{6}$$

in which $\mathbf{E}$ is the complex electric field and $\varepsilon''$ is the imaginary part of the dielectric function. The absorptance of a certain volume can be obtained from the ratio of the power dissipated inside it over the incident power:[25]

$$\alpha = \frac{\iiint w(x, z)\mathrm{d}V}{(1/2)c_0\varepsilon_0|\mathbf{E}_{inc}|^2 A\cos\theta} \tag{7}$$

Here, the denominator is the power of the incident plane wave on an area $A$ at incidence angle $\theta$. Therefore, by evaluating eq 7 in graphene, one is able to separate the absorptance of graphene from the absorptance of the whole graphene-covered structure. A detailed discussion about incorporating the equations with traditional RCWA algorithm to calculate the absorptance is given in another work.[26]

**LC Circuit Model.** For the gratings considered in this work, the two walls and the bottom of the trench provide the inductance in the circuit, and the vacuumed gap in the trench


DOI: 10.1021/acsphotonics.5b00410
ACS Photonics 2015, 2, 1611−1618

serves as a capacitor. The inductance of the metal trench walls, $L_{Ag}$, is modeled as[32,46]

$$L_{Ag} = -\frac{2h + b}{\varepsilon_0 \omega^2 l \delta} \frac{\varepsilon'_{Ag}}{(\varepsilon'^2_{Ag} + \varepsilon''^2_{Ag})} + \mu_0 \frac{hb}{l} \quad (8)$$

where $\mu_0$ is the permeability of vacuum, and $\varepsilon'_{Ag}$ and $\varepsilon''_{Ag}$ are the real and imaginary parts of the dielectric function of Ag, respectively. $\delta = \lambda/2\pi\kappa$ is the penetration depth of the electric field, in which $\kappa$ is the extinction coefficient. $l$ is the length in the $y$-direction that can be set to unity for one-dimensional gratings. Similarly, the inductance from graphene ribbon is

$$L_{rib} = -\mathrm{Im}\left(\frac{r}{\omega l \sigma_s}\right) \quad (9)$$

Im means taking the imaginary part. Meanwhile, the capacitance of the vacuum in the trench can be approximated by[32]

$$C = c' \varepsilon_0 \frac{hl}{b} \quad (10)$$

where $c'$ is a numerical factor and assumed to be 0.5 to account for the nonuniform charge distribution along the trench walls.[32,46] The resonance condition can be then predicted by the natural frequency of the equivalent LC circuit:[32]

$$\omega = \frac{1}{\sqrt{LC}} \quad (11)$$

The inductance $L$ is $L_{Ag}$ for plain gratings and equals to $L_{Ag}L_{rib}/(L_{Ag} + L_{rib})$ for the ribbon-covered structure since the two inductors are in parallel. Details of the LC model are given in the Supporting Information.

## ■ ASSOCIATED CONTENT

### Supporting Information

The Supporting Information is available free of charge on the ACS Publications website at DOI: 10.1021/acsphotonics.5b00410.

Detailed discussion of the LC circuit model, the effect of lowering the graphene ribbons, small elevation of the graphene ribbons, and the interband transitions on the coupled resonance are given (PDF).

## ■ AUTHOR INFORMATION


### Corresponding Author

*E-mail: zhuomin.zhang@me.gatech.edu.


### Notes

The authors declare no competing financial interest.

## ■ ACKNOWLEDGMENTS

The research is mainly supported by the National Science Foundation (CBET-1235975). Z.M.Z. would also like to thank the support of the U.S. Department of Energy, Office of Science, Basic Energy Sciences (DE-FG02-06ER46343).

## ■ REFERENCES


(1) García de Abajo, F. J. Graphene Plasmonics: Challenges and Opportunities. *ACS Photonics* **2014**, *1*, 135−152.

(2) Jablan, M.; Soljacic, M.; Buljan, H. Plasmons in Graphene: Fundamental Properties and Potential Applications. *Proc. IEEE* **2013**, *101*, 1689−1704.

(3) Low, T.; Avouris, P. Graphene Plasmonics for Terahertz to Mid-Infrared Applications. *ACS Nano* **2014**, *8*, 1086−1101.

(4) Grigorenko, A. N.; Polini, M.; Novoselov, K. S. Graphene Plasmonics. *Nat. Photonics* **2012**, *6*, 749−758.

(5) Ju, L.; Geng, B.; Horng, J.; Girit, C.; Martin, M.; Hao, Z.; Bechtel, H. A.; Liang, X.; Zettl, A.; Shen, Y. R.; Wang, F. Graphene Plasmonics for Tunable Terahertz Metamaterials. *Nat. Nanotechnol.* **2011**, *6*, 630−634.

(6) Chugh, S.; Man, M.; Chen, Z.; Webb, K. J. Ultra-Dark Graphene Stack Metamaterials. *Appl. Phys. Lett.* **2015**, *106*, 061102.

(7) Alaee, R.; Farhat, M.; Rockstuhl, C.; Lederer, F. A Perfect Absorber Made of a Graphene Micro-Ribbon Metamaterial. *Opt. Express* **2012**, *20*, 28017−28024.

(8) Piper, J. R.; Fan, S. Total Absorption in a Graphene Monolayer in the Optical Regime by Critical Coupling with a Photonic Crystal Guided Resonance. *ACS Photonics* **2014**, *1*, 347−353.

(9) Liu, B.; Liu, Y.; Shen, S. Thermal Plasmonic Interconnects in Graphene. *Phys. Rev. B: Condens. Matter Mater. Phys.* **2014**, *90*, 195411.

(10) Brar, V. W.; Jang, M. S.; Sherrott, M.; Lopez, J. J.; Atwater, H. A. Highly Confined Tunable Mid-Infrared Plasmonics in Graphene Nanoresonators. *Nano Lett.* **2013**, *13*, 2541−2547.

(11) Nikitin, A. Y.; Guinea, F.; Garcia-Vidal, F. J.; Martin-Moreno, L. Surface Plasmon Enhanced Absorption and Suppressed Transmission in Periodic Arrays of Graphene Ribbons. *Phys. Rev. B: Condens. Matter Mater. Phys.* **2012**, *85*, 081405.

(12) Strait, J. H.; Nene, P.; Chan, W.-M.; Manolatou, C.; Tiwari, S.; Rana, F.; Kevek, J. W.; McEuen, P. L. Confined Plasmons in Graphene Microstructures: Experiments and Theory. *Phys. Rev. B: Condens. Matter Mater. Phys.* **2013**, *87*, 241410.

(13) Yan, H.; Low, T.; Zhu, W.; Wu, Y.; Freitag, M.; Li, X.; Guinea, F.; Avouris, P.; Xia, F. Damping Pathways of Mid-Infrared Plasmons in Graphene Nanostructures. *Nat. Photonics* **2013**, *7*, 394−399.

(14) Yi, S.; Zhou, M.; Shi, X.; Gan, Q.; Zi, J.; Yu, Z. A Multiple-Resonator Approach for Broadband Light Absorption in a Single Layer of Nanostructured Graphene. *Opt. Express* **2015**, *23*, 10081−10090.

(15) Koppens, F. H. L.; Chang, D. E.; García de Abajo, F. J. Graphene Plasmonics: A Platform for Strong Light−Matter Interactions. *Nano Lett.* **2011**, *11*, 3370−3377.

(16) Yan, H.; Li, X.; Chandra, B.; Tulevski, G.; Wu, Y.; Freitag, M.; Zhu, W.; Avouris, P.; Xia, F. Tunable Infrared Plasmonic Devices Using Graphene/Insulator Stacks. *Nat. Nanotechnol.* **2012**, *7*, 330−334.

(17) Fang, Z.; Wang, Y.; Schlather, A. E.; Liu, Z.; Ajayan, P. M.; García de Abajo, F. J.; Nordlander, P.; Zhu, X.; Halas, N. J. Active Tunable Absorption Enhancement with Graphene Nanodisk Arrays. *Nano Lett.* **2014**, *14*, 299−304.

(18) Fallahi, A.; Perruisseau-Carrier, J. Design of Tunable Biperiodic Graphene Metasurfaces. *Phys. Rev. B: Condens. Matter Mater. Phys.* **2012**, *86*, 195408.

(19) Gao, W.; Shi, G.; Jin, Z.; Shu, J.; Zhang, Q.; Vajtai, R.; Ajayan, P. M.; Kono, J.; Xu, Q. Excitation and Active Control of Propagating Surface Plasmon Polaritons in Graphene. *Nano Lett.* **2013**, *13*, 3698−3702.

(20) Jang, M. S.; Brar, V. W.; Sherrott, M. C.; Lopez, J. J.; Kim, L.; Kim, S.; Choi, M.; Atwater, H. A. Tunable Large Resonant Absorption in a Midinfrared Graphene Salisbury Screen. *Phys. Rev. B: Condens. Matter Mater. Phys.* **2014**, *90*, 165409.

(21) Thareja, V.; Kang, J.-H.; Yuan, H.; Milaninia, K. M.; Hwang, H. Y.; Cui, Y.; Kik, P. G.; Brongersma, M. L. Electrically Tunable Coherent Optical Absorption in Graphene with Ion Gel. *Nano Lett.* **2015**, *15*, 1570−1576.

(22) Echtermeyer, T. J.; Britnell, L.; Jasnos, P. K.; Lombardo, A.; Gorbachev, R. V.; Grigorenko, A. N.; Geim, A. K.; Ferrari, A. C.; Novoselov, K. S. Strong Plasmonic Enhancement of Photovoltage in Graphene. *Nat. Commun.* **2011**, *2*, 458.

(23) Fang, Z.; Liu, Z.; Wang, Y.; Ajayan, P. M.; Nordlander, P.; Halas, N. J. Graphene-Antenna Sandwich Photodetector. *Nano Lett.* **2012**, *12*, 3808−3813.




DOI: 10.1021/acsphotonics.5b00410
*ACS Photonics* 2015, 2, 1611−1618

(24) Yao, Y.; Shankar, R.; Rauter, P.; Song, Y.; Kong, J.; Loncar, M.; Capasso, F. High-Responsivity Mid-Infrared Graphene Detectors with Antenna-Enhanced Photocarrier Generation and Collection. *Nano Lett.* **2014**, *14*, 3749−3754.
(25) Zhao, B.; Zhao, J. M.; Zhang, Z. M. Enhancement of Near-Infrared Absorption in Graphene with Metal Gratings. *Appl. Phys. Lett.* **2014**, *105*, 031905.
(26) Zhao, B.; Zhao, J. M.; Zhang, Z. M. Resonance Enhanced Absorption in a Graphene Monolayer Using Deep Metal Gratings. *J. Opt. Soc. Am. B* **2015**, *32*, 1176−1185.
(27) Cai, Y.; Zhu, J.; Liu, Q. H. Tunable Enhanced Optical Absorption of Graphene Using Plasmonic Perfect Absorbers. *Appl. Phys. Lett.* **2015**, *106*, 043105.
(28) Papasimakis, N.; Luo, Z.; Shen, Z. X.; De Angelis, F.; Di Fabrizio, E.; Nikolaenko, A. E.; Zheludev, N. I. Graphene in a photonic metamaterial. *Opt. Express* **2010**, *18*, 8353−8359.
(29) Gilbertson, A. M.; Francescato, Y.; Roschuk, T.; Shautsova, V.; Chen, Y.; Sidiropoulos, T. P. H.; Hong, M.; Giannini, V.; Maier, S. A.; Cohen, L. F.; Oulton, R. F. Plasmon-Induced Optical Anisotropy in Hybrid Graphene−Metal Nanoparticle Systems. *Nano Lett.* **2015**, *15*, 3458−3464.
(30) Li, Z.; Yu, N. Modulation of Mid-Infrared Light Using Graphene-Metal Plasmonic Antennas. *Appl. Phys. Lett.* **2013**, *102*, 131108.
(31) Alonso-González, P.; Nikitin, A. Y.; Golmar, F.; Centeno, A.; Pesquera, A.; Vélez, S.; Chen, J.; Navickaite, G.; Koppens, F.; Zurutuza, A.; Casanova, F.; Hueso, L. E.; Hillenbrand, R. Controlling Graphene Plasmons with Resonant Metal Antennas and Spatial Conductivity Patterns. *Science* **2014**, *344*, 1369−1373.
(32) Zhao, B.; Zhang, Z. M. Study of Magnetic Polaritons in Deep Gratings for Thermal Emission Control. *J. Quant. Spectrosc. Radiat. Transfer* **2014**, *135*, 81−89.
(33) Falkovsky, L. A. Optical Properties of Graphene. *J. Phys. Conf. Ser.* **2008**, *129*, 012004.
(34) Zhao, B.; Wang, L. P.; Shuai, Y.; Zhang, Z. M. Thermophotovoltaic Emitters Based on a Two-Dimensional Grating/Thin-Film Nanostructure. *Int. J. Heat Mass Transfer* **2013**, *67*, 637−645.
(35) Engheta, N. Circuits with Light at Nanoscales: Optical Nanocircuits Inspired by Metamaterials. *Science* **2007**, *317*, 1698−1702.
(36) Sakurai, A.; Zhao, B.; Zhang, Z. M. Resonant Frequency and Bandwidth of Metamaterial Emitters and Absorbers Predicted By an RLC Circuit Model. *J. Quant. Spectrosc. Radiat. Transfer* **2014**, *149*, 33−40.
(37) Vakil, A.; Engheta, N. Transformation Optics Using Graphene. *Science* **2011**, *332*, 1291−1294.
(38) Chen, J.; Nesterov, M. L.; Nikitin, A. Y.; Thongrattanasiri, S.; Alonso-González, P.; Slipchenko, T. M.; Speck, F.; Ostler, M.; Seyller, T.; Crassee, I.; Koppens, F. H. L.; Martin-Moreno, L.; García de Abajo, F. J.; Kuzmenko, A. B.; Hillenbrand, R. Strong Plasmon Reflection at Nanometer-Size Gaps in Monolayer Graphene on SiC. *Nano Lett.* **2013**, *13*, 6210−6215.
(39) Garcia-Pomar, J. L.; Nikitin, A. Y.; Martin-Moreno, L. Scattering of Graphene Plasmons by Defects in the Graphene Sheet. *ACS Nano* **2013**, *7*, 4988−4994.
(40) Nikitin, A. Y.; Low, T.; Martin-Moreno, L. Anomalous Reflection Phase of Graphene Plasmons and Its Influence on Resonators. *Phys. Rev. B: Condens. Matter Mater. Phys.* **2014**, *90*, 041407.
(41) Du, L.; Tang, D.; Yuan, X. Edge-Reflection Phase Directed Plasmonic Resonances on Graphene Nano-Structures. *Opt. Express* **2014**, *22*, 22689−22698.
(42) Wang, H.; Yang, Y.; Wang, L. P. Infrared Frequency-Tunable Coherent Thermal Sources. *J. Opt.* **2015**, *17*, 045104.
(43) http://zhang-nano.gatech.edu/.
(44) Khavasi, A. Fast Convergent Fourier Modal Method for The Analysis of Periodic Arrays of Graphene Ribbons. *Opt. Lett.* **2013**, *38*, 3009−3012.
(45) Zhao, J. M.; Zhang, Z. M. Electromagnetic Energy Storage and Power Dissipation in Nanostructures. *J. Quant. Spectrosc. Radiat. Transfer* **2015**, *151*, 49−57.
(46) Wang, L. P.; Zhang, Z. M. Phonon-Mediated Magnetic Polaritons in the Infrared Region. *Opt. Express* **2011**, *19*, A126−A135.


DOI: 10.1021/acsphotonics.5b00410
*ACS Photonics* 2015, 2, 1611−1618